Check for updates

Geophysical Research Letters

RESEARCH LETTER
10.1029/2023GL104901

Systematic Detection of Short-Term Slow Slip Events in Southcentral Alaska

Yutaro Okada[1] and **Takuya Nishimura**[2]

[1]Graduate School of Science, Kyoto University, Kyoto, Japan, [2]Disaster Prevention Research Institute, Kyoto University, Kyoto, Japan

Key Points:

- Systematic detection identified 31 short-term slow slip events in southcentral Alaska from 14 years of Global Navigation Satellite System data
- The slow slips were located at a depth from 35 to 45 km, particularly in the region where the Yakutat microplate subducts
- The short-term slow slips overlap the source areas of the long-term slow slips and the 1964 Alaska earthquake afterslip

Supporting Information:

Supporting Information may be found in the online version of this article.

Correspondence to:

Y. Okada,
okada.yutarou.24r@st.kyto-u.ac.jp

Citation:

Okada, Y., & Nishimura, T. (2023). Systematic detection of short-term slow slip events in southcentral Alaska. *Geophysical Research Letters*, *50*, e2023GL104901. https://doi.org/10.1029/2023GL104901

Received 16 JUN 2023
Accepted 15 AUG 2023

Author Contributions:

Conceptualization: Yutaro Okada
Formal analysis: Yutaro Okada
Funding acquisition: Takuya Nishimura
Methodology: Yutaro Okada
Supervision: Takuya Nishimura
Writing – original draft: Yutaro Okada
Writing – review & editing: Takuya Nishimura

© 2023. The Authors.
This is an open access article under the terms of the Creative Commons Attribution License, which permits use, distribution and reproduction in any medium, provided the original work is properly cited.

Abstract Slow slip events (SSEs) are important for the slip budget along a megathrust fault. Although the recurrence of weeks-long short-term SSEs (S-SSEs) in southcentral Alaska has been suggested, a large amount of noise prevented us from detecting discrete events. We applied a systematic detection method to Global Navigation Satellite System data and detected 31 S-SSEs during the 14-year analysis period. The events mainly occurred at a depth from 35 to 45 km at a down-dip extension of the 1964 Alaska earthquake, and the active clusters correlated with the region of the subducting Yakutat microplate. A large cumulative slip of S-SSEs indicated a significant contribution to stress transfer along the plate interface, and its source area spatially coincided with that of the long-term SSEs and the afterslip of the 1964 earthquake. Large and recurrent S-SSEs are key phenomena for understanding interplate slip kinematics in this region.

Plain Language Summary Slow and transient fault slips, called slow slip events (SSEs), are important phenomena accommodating plate motion during interseismic periods. However, detecting SSEs, especially short-term SSEs (S-SSEs) that last from days to weeks, is sometimes difficult because of their weak signals. In southcentral Alaska, previous studies have detected S-SSEs as several discrete events synchronizing with tectonic tremors, but their spatiotemporal distribution and the features of their magnitude and duration are still unclear. We applied a systematic detection method to 14 years of daily Global Navigation Satellite System position data and successfully detected 31 S-SSEs. We found two major groups of S-SSEs (S-SSE clusters) at a depth from 35 to 45 km, which corresponds to a deeper extension of the source of the 1964 Alaska earthquake. These clusters are located in the region where the Yakutat microplate subducts. Maximum cumulative slip reaches 0.27 and 0.43 m in the western and eastern clusters, respectively, and it suggests that S-SSEs contribute to the reduction of the large amount of interplate slip in their source areas.

1. Introduction

Slow slip events (SSEs) are aseismic transient slips that are geodetically observed in worldwide fault zones (e.g., Dragert et al., 2001; Hirose et al., 1999; Ohzono et al., 2015; Rousset, Bürgmann, & Campillo, 2019). Previous studies (e.g., Fu et al., 2015; Obara et al., 2004; Wallace, 2020) suggest a wide variety of SSE characteristics including magnitude, duration, source depth, tectonic setting of source regions, and so on. The duration of SSEs is sometimes used to categorize these events into long-term SSEs (L-SSEs) that last several months to years and short-term SSEs (S-SSEs) that continue from several days to weeks (Dragert et al., 2001; Hirose et al., 1999). S-SSEs in subduction zones, including the Cascadia, Nankai, and Mexican subduction zones (Frank et al., 2015; Obara et al., 2004; Rogers & Dragert, 2003), often synchronize with seismological "slow" earthquakes (Beroza & Ide, 2011) including tectonic tremors (Obara, 2002), and referred Episodic Tremor and Slip (ETS). However, SSEs without apparent slow earthquakes have also been reported in the regions including the Boso Peninsula and the Ryukyu Islands in Japan and La Plata Island in Ecuador (Nishimura, 2014; Ozawa et al., 2003; Vallée et al., 2013). It is also known that a tremor-less slow slip was observed during an S-SSE episode in the regions of ETS events (Obara & Sekine, 2009; Wech & Bartlow, 2014). These variations highlight the importance of further SSE detections in different tectonic regions to understand the regional and universal characteristics of SSEs and slow earthquakes. Studying SSEs also helps us understand the slip budget in the SSE source areas, which are often located around the rupture area of large earthquakes.

The Pacific plate and Yakutat microplate subduct beneath the North America plate in southcentral Alaska. The *M* 9.2 Alaska earthquake occurred in 1964 (e.g., Christensen & Beck, 1994) and its postseismic deformation is still ongoing (e.g., Suito & Freymueller, 2009). Two L-SSEs occurred in Upper Cook Inlet (UCI): the first in 1998–

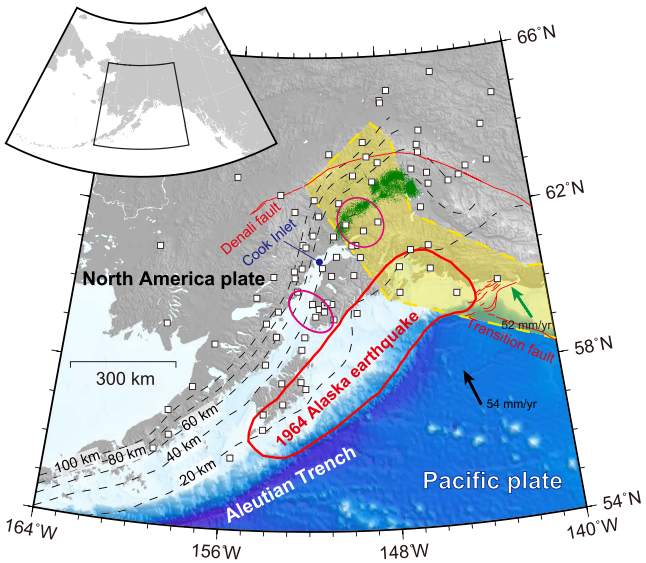

Figure 1. Tectonic setting and station distribution. Black dashed lines, red solid lines, pink ellipses, green dots, the red polygon, and the yellow polygon represent iso-depth contours of the subducting plate interface (Hayes et al., 2018), active faults (U.S. Geological Survey & Alaska Department of Natural Resources, accessed December 2021), L-SSEs (e.g., Fu et al., 2015; Ohta et al., 2006; Wei et al., 2012), tectonic tremors (Wech, 2016), the 1964 Alaska earthquake rupture area (Christensen & Beck, 1994), and the Yakutat microplate (Eberhart-Phillips et al., 2006), respectively. The black and green arrows show the plate motion of the Pacific plate (Plattner et al., 2007) and the Yakutat microplate (Elliott et al., 2010) relative to the North America plate, respectively. White squares represent the Global Navigation Satellite System stations used in this study.

2001 and the second in 2009–2013 (Fu et al., 2015; Ohta et al., 2006), while three were observed in Lower Cook Inlet (LCI): 1992–2004, 2010–2012, and 2016–2017 (H. Li et al., 2018; S. Li et al., 2016; Wei et al., 2012) (Figure 1). L-SSEs occurred at the down-dip extension of the rupture area of the 1964 Alaska earthquake (e.g., Christensen & Beck, 1994; Ohta et al., 2006) and correspond to the source area of the afterslip of the 1964 earthquake (Figure 1) (e.g., Suito & Freymueller, 2009). Tectonic tremors in southcentral Alaska have been reported since the late 2000s (Schwartz & Rokosky, 2007). Their source area corresponds to the subducting Yakutat microplate and overlaps with that of UCI L-SSEs (e.g., Wech, 2016) (Figure 1).

Rousset, Fu et al. (2019) discovered an M_w 6.9 S-SSE lasting 27 days in southcentral Alaska for the first time. This S-SSE began in early September 2010, after the onset of the 2009–2013 UCI L-SSE, and the slip propagated from east to west, corresponding to the migration of tremors. Those authors also found that the cumulative displacements during tremor bursts showed a strain release signal and indicated that many S-SSEs synchronizing with tremor actually occur in UCI. Weerasinghe and Fu (2021) detected additional S-SSEs that corresponded to tremors. However, spatiotemporal variations in S-SSE recurrence and the general features of the source parameters are still unclear.

Here, we attempted to systematically detect S-SSEs in southcentral Alaska using Global Navigation Satellite System (GNSS) data and investigate their activity. Systematic detection enables us to find small S-SSE signals hidden by noise without a tremor catalog, even if the GNSS network is relatively sparse. We also attempted to determine the relationship between the detected S-SSEs and tremors, L-SSEs, and the 1964 Alaska earthquake.

2. Data and Detection Method

2.1. Data and Preprocesses

We used the daily coordinates of 86 GNSS stations provided by the Nevada Geodetic Laboratory (Blewitt et al., 2018; http://geodesy.unr.edu/, accessed in July 2021) (Figure 1). We used coordinates for the period from April 2007 to March 2021, in which the number of available GNSS stations is large enough for our detection analysis. As preprocessing step, we removed signals relating to large earthquakes, seasonal oscillations, and common-mode errors (Text S1 and Figure S1 in Supporting Information S1).

2.2. Detection Method

We modified the S-SSE systematic detection method (Okada et al., 2022) and applied it to the preprocessed GNSS timeseries. First, we computed the correlation coefficients between a synthetic template and the horizontal components of the GNSS data that was detrended using the 365-day moving average while shifting the 181-day time window. The synthetic template is the summation of a ramp with a 3-day duration, representing an SSE signal, and a linear function to fix no displacement at either end of the template.

Second, we calculated the weighted averages of the correlation coefficients (e.g., Rousset et al., 2017), expressed as:

$$C^f(t) = \frac{\sum_{s=1}^{N}\sum_{i=1}^{2} G^f_{s,i} C_{s,i}(t)}{\sum_{s=1}^{N}\sum_{i=1}^{2} \left| G^f_{s,i} \right|}, \quad (1)$$

19448007, 2023, 17, Downloaded from https://agupubs.onlinelibrary.wiley.com/doi/10.1029/2023GL104901 by Cochrane Japan, Wiley Online Library on [29/11/2023]. See the Terms and Conditions (https://onlinelibrary.wiley.com/terms-and-conditions) on Wiley Online Library for rules of use; OA articles are governed by the applicable Creative Commons License

19448007, 2023, 17, Downloaded from https://agupubs.onlinelibrary.wiley.com/doi/10.1029/2023GL104901 by Cochrane Japan, Wiley Online Library on [29/11/2023]. See the Terms and Conditions (https://onlinelibrary.wiley.com/terms-and-conditions) on Wiley Online Library for rules of use; OA articles are governed by the applicable Creative Commons License

where $C_{s,i}(t)$ is the correlation coefficient of the i th component at station s calculated at time t. The weighted average $C^f(t)$ and weight $G^f_{s,i}$ is calculated for each sub-fault f on the plate interface (Hayes et al., 2018). The weight is defined as:

$$G^f_{s,i} = \frac{g^f_{s,i}}{\max\left(\left|g^f_{s,i}\right|\right)}, \tag{2}$$

where $g^f_{s,i}$ is the displacement of the i th component at station s caused by a unit slip, which is parallel to the relative plate motion (N160°E) (DeMets et al., 2010), at sub-fault f. We assumed sub-faults at depths from 10 to 80 km (Figure S2 in Supporting Information S1) and computed displacements using a dislocation model for an elastic half-space (Okada, 1992). The weighted average of correlation coefficients changes with space and time and sometimes exhibits their peak value near tremor epicenters (Wech, 2016). It demonstrates that the weighted average of correlation coefficients can be a good index representing small SSE signals associated with tectonic tremors (Figure S3a in Supporting Information S1). Third, we extracted the spatiotemporal peaks of the weighted averages. We extracted peaks larger than the sum of the average and one sigma from the weighted averages for each sub-fault. We then chose the maximum peaks within 150 km (Figure S3a in Supporting Information S1) and 41 days (Figure S3b in Supporting Information S1) and regarded the sub-fault and date recording the maximum peak as the initial location of the fault model and the middle date of the candidate event of the S-SSEs. The S-SSE activity in this region has not been evident yet, and tremor catalogs have been limited to a specific region (e.g., northeast of Cook Inlet) and period. Thus, we picked up as many candidates of potential SSEs as possible using the relatively loose thresholds. Because of the loose selection, the candidates include many non-SSE events as well as some actual SSEs, and we need further categorization for accurate SSE detection.

Fourthly, we estimated the preliminary duration of candidate events to reduce computational cost. We stacked 181-day horizontal GNSS coordinates weighted by the predicted displacement $g^f_{s,i}$ and the noise level of the coordinates. We then fitted a linear function with and without a ramp and calculated the difference in the Akaike Information Criterion (Akaike, 1974) between the two functions (ΔAIC). We performed this process while changing the duration of the ramp from 1 to 121 days and adopted the duration for the minimum ΔAIC as the preliminary duration of the candidate events (Rousset, Bürgmann, & Campillo, 2019). The following fault model and duration estimation process were applied between $\pm$20 days of the preliminary duration. Details of this stacking procedure are provided in Text S2 in Supporting Information S1. Fifthly, we estimated the rectangular fault model (Okada, 1992) of the candidate events for each duration (Text S3 in Supporting Information S1). We assessed the estimation result of the fault model using the reduction of chi-square ($\Delta\chi^2$), which is an index that evaluates the fit of the fault model (Text S3 in Supporting Information S1) (e.g., Okada et al., 2022). Sixthly, we estimated the duration of candidate events using the same method as the estimation of the preliminary duration. In the duration estimation process, we weighted the coordinates by the displacements calculated from the estimated fault model for each duration instead of the displacements $g^f_{s,i}$ predicted from the assumed sub-fault. We adopted the duration with minimum ΔAIC and the fault model corresponding to the duration as those of the candidate.

Finally, we categorized the candidate events into S-SSEs based on the estimation results of the fault models and duration. The criteria are as follows: (a) the slip azimuth of the fault model (strike minus rake) is within $\pm$40° of the relative plate motion (N160°E) (DeMets et al., 2010); (b) the minimum ΔAIC calculated for the duration estimation process is $-$60 or less; and (c) $\Delta\chi^2$ calculated in the fault model estimation process is 200 or more. In addition, we also categorized the candidate events which satisfy criteria (a) and (b) but $\Delta\chi^2$ is between 100 and 200 into potential transient events (PTEs). This category includes both possible small SSEs and false detected events. The criterion for ΔAIC and $\Delta\chi^2$ was decided by trial-and-error while checking the signal-to-noise ratio of the stacked timeseries, the fitting between observed and calculated displacement field, and coinciding tremors (Wech, 2016). We verified that the spatial pattern of the detected events does not significantly change depending on the different $\Delta\chi^2$ values (Text S3 and Figure S4 in Supporting Information S1).

3. Result and Discussion

3.1. General Characteristics of the Detected S-SSEs

We successfully detected 31 S-SSEs and 20 PTEs during the 14-year analysis period. Most of the detected S-SSEs are zonally distributed at a depth from 35 to 45 km, which is the down-dip extension of the megathrust rupture

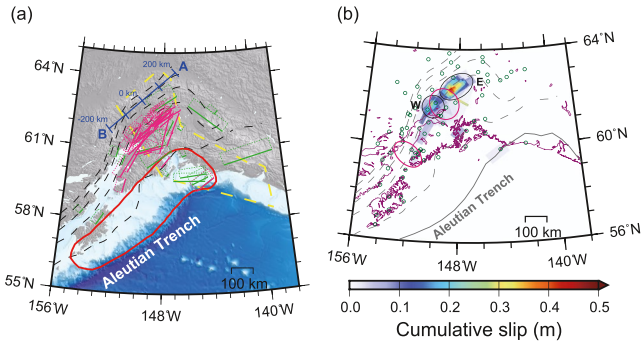

Figure 2. Spatial distribution of the detected S-SSEs. Black and gray dashed lines represent iso-depth contours of the subducting plate interface (Hayes et al., 2018). (a) Spatial distribution of rectangular fault models of the detected S-SSEs. Pink and green rectangles show the fault models of SSEs and PTEs, respectively. The red solid line and broken yellow line represent the rupture area of the 1964 Alaska earthquake (Christensen & Beck, 1994) and the Yakutat microplate (Eberhart-Phillips et al., 2006), respectively. The blue length scale is the projection line used in Figure 4. (b) Spatial distribution of the cumulative slip for S-SSEs. A solid line and green circles represent a plate boundary (Bird, 2003) and Global Navigation Satellite System stations. Pink and black ellipses show the approximate location of the L-SSEs (e.g., Fu et al., 2015; Ohta et al., 2006; Wei et al., 2012) and western (W) and eastern (E) SSE clusters, respectively.

zone (Christensen & Beck, 1994) (Figure 2, Figures S4, and S5 and Table S5 in Supporting Information S1). The depth of S-SSE occurrence and zonal distribution along a direction parallel to the trench are similar to those in the Cascadia and Nankai subduction zones (e.g., Michel et al., 2019a; Nishimura et al., 2013). One S-SSE was detected in near the Trench (Figure 2a), but this event is less reliable because only one station recorded the displacement indicating reverse faulting.

Most of the detected S-SSEs were located northeast of Cook Inlet, though several S-SSEs were detected on the Kenai Peninsula and Kodiak Island (Figure 2). The region of many S-SSEs corresponds to the region where the Yakutat microplate subducts (Eberhart-Phillips et al., 2006), similar to the source region of tectonic tremors (Wech, 2016) (Figures 1 and 2a). Wech (2016) indicated that the fluid-rich layer at the Yakutat microplate interface (Kim et al., 2014) facilitates tremors, and a recent numerical simulation of the thermal structure in this region supports this hypothesis (Iwamoto et al., 2022). Our detection shows a clear spatial correlation between S-SSEs and the Yakutat microplate, and we speculate that the fluid-rich layer also enhances an S-SSE activity in southcentral Alaska.

Cumulative slip for S-SSEs shows two spots with high cumulative slip northeast of Cook Inlet (Figure 2b). We hereafter call these spots clusters. A peak of cumulative slip in the western and eastern clusters is up to 0.27 m (~19 mm/yr) and 0.43 m (~31 mm/yr) over the 14 years (Figure 2b), respectively. They are equivalent to approximately 37% and 60% of the relative plate motion rate of the Yakutat microplate (52 mm/yr) (Elliott et al., 2010). Active S-SSEs are located in the transition zone between the fully coupling and fully creeping zones (S. Li et al., 2016) and they may regularly transfer stress into the up-dip coupled region. We also calculated the average slip rate of S-SSEs (Figure S6b in Supporting Information S1), which is the division of the cumulative slip (Figure 2b) by the cumulative duration (Figure S6a in Supporting Information S1). It is about 1 mm/day, similar to that in the Nankai subduction zone (Okada et al., 2022).

The moment magnitude assuming a rigidity of 50 GPa and the duration of S-SSEs and PTEs mainly range from M_w 6.2 to 6.7 and from 1 to 50 days, respectively (Figures S7a and S7b in Supporting Information S1). We suggest that the lowest limit detectability in this region is M_w 6.3, because the mode value of the frequency distribution of S-SSEs' magnitude (Figure S7 in Supporting Information S1) corresponds to the completeness magnitude of an earthquake catalog. Although the number of detected S-SSEs and the range of magnitude is limited, the seismic moment of the S-SSEs appears to be proportional to their duration (Ide et al., 2007) (Figure S7c in Supporting Information S1), unlike the result by Michel et al. (2019b) which suggested that the seismic moment of S-SSEs in Cascadia is proportional to the cube of their duration. We infer that the relationship between seismic moment and duration of S-SSE has regionality, although we require further validation to determine which relationship better fits the S-SSEs in southcentral Alaska.

3.2. Individual Events

We show fault models with observed and calculated displacements for all detected events (Figures S9–S59 in Supporting Information S1) and picked up notable events in Figure 3. The 2010 September S-SSE was detected by both Rousset, Fu et al. (2019) and our study (Figure 3a). The fault location is not significantly different between the two studies, whereas the estimated magnitude and duration is less in our study than in those of Rousset, Fu et al. (2019). Although the differences between the assumed plate interface model and slip inversion strategy possibly affected the estimation, a wider station distribution compared with that of Rousset, Fu et al. (2019) is the main reason for the smaller moment than the previous one. In late September 2010, coherent southward displacements widely appeared around southcentral Alaska (Figure S8 in Supporting Information S1). We regarded these translational displacements as noise and removed them by applying the spatial filter (Wdowinski et al., 1997) in the preprocessing (Text S1 in Supporting Information S1).

We detected the S-SSE in June 2014 (Figure 3b), which synchronized with tectonic tremors (Wech, 2016) as similar to the September 2010 S-SSE, after the end of the 2009–2013 L-SSE. Our results show that S-SSEs

19448007, 2023, 17, Downloaded from https://agupubs.onlinelibrary.wiley.com/doi/10.1029/2023GL104901 by Cochrane Japan, Wiley Online Library on [29/11/2023]. See the Terms and Conditions (https://onlinelibrary.wiley.com/terms-and-conditions) on Wiley Online Library for rules of use; OA articles are governed by the applicable Creative Commons License

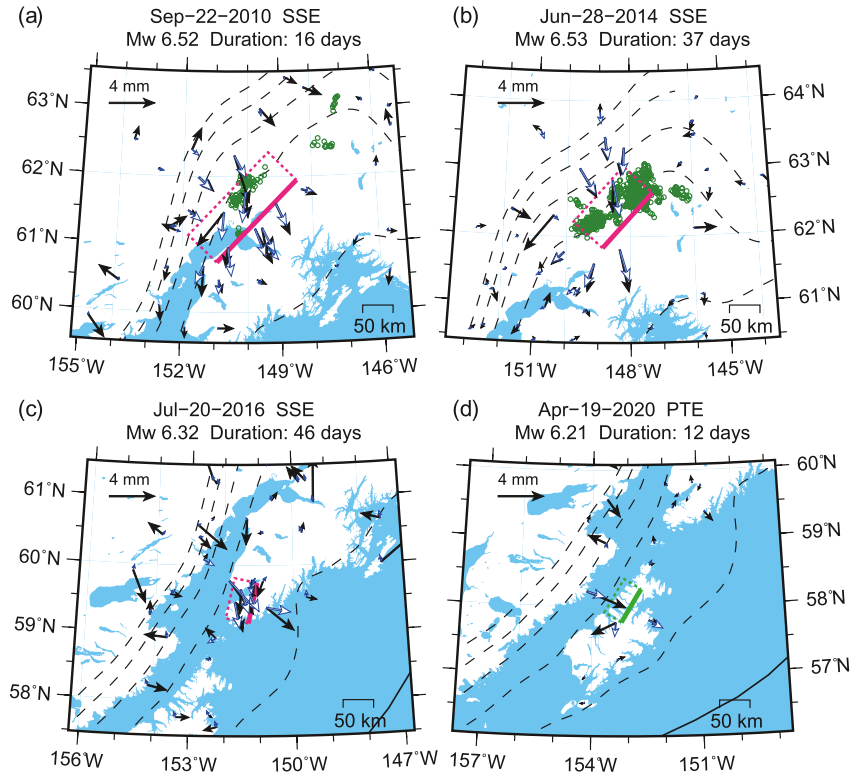

Figure 3. Examples of the detected events. Colored rectangles, green dots, black solid arrows, and blue open arrows represent the estimated fault model, tectonic tremors (Wech, 2016), observed displacements, and calculated displacements, respectively. Black dashed and solid lines show iso-depth contours of the subducting plate interface with an interval of 20 km (Hayes et al., 2018) and the plate boundary (Bird, 2003), respectively. (a) September 2010 S-SSE. (b) June 2014 S-SSE. (c) July 2016 S-SSE. (d) April 2020 PTE.

recurred in southcentral Alaska, regardless of the occurrence of the L-SSEs, as suggested by previous studies (e.g., Rousset, Fu et al., 2019).

Although station density does not significantly differ from that northeast of Cook Inlet, our systematic detection procedure identified only three S-SSEs in the Kenai Peninsula (Figure 2a). Because two S-SSEs (Figure 3c and S42 in Supporting Information S1) were detected during the period of the 2016–2017 LCI L-SSE (e.g., H. Li et al., 2018), we believe that we recognized the slip acceleration period of the L-SSE as an S-SSE. We speculate that the contrast of S-SSE activity in the Kenai Peninsula and northeast of Cook Inlet is attributed to different subducting plates, as discussed in Section 3.1.

We detected two PTEs on Kodiak Island and the Alaska Peninsula (Figure 2a). We interpret the April 2020 PTE as an SSE based on coherent displacement at multiple stations (Figure 3d). Future expansion of onshore and offshore geodetic measurements will help us detect further smaller events.

3.3. Spatiotemporal Activity of S-SSEs

We investigated the spatiotemporal activity of the detected S-SSEs and PTEs. Here, we focused on the region northeast of Cook Inlet and at a depth greater than 20 km because of the high activity of S-SSEs and tremors observed in that area (Wech, 2016) (Figures 2a and 4). We found that many S-SSEs and three PTEs spatiotemporally synchronized with tremors, especially after the upgrade of a seismic network (Wech, 2016). Our results showed that the S-SSEs northeast of Cook Inlet are ETS-type events, similar to the SSEs in Cascadia, Nankai, and Mexico (Obara et al., 2004; Rogers & Dragert, 2003; Rousset et al., 2017). However, the S-SSE activity at a distance of ≥100 km, where tremors continuously occur (Wech, 2016), is less frequent than that in a more western area (Figure 4). We infer that the current geodetic observation cannot detect small and frequent S-SSEs with short recurrence intervals in this region.

19448007, 2023, 17, Downloaded from https://agupubs.onlinelibrary.wiley.com/doi/10.1029/2023GL104901 by Cochrane Japan, Wiley Online Library on [29/11/2023]. See the Terms and Conditions (https://onlinelibrary.wiley.com/terms-and-conditions) on Wiley Online Library for rules of use; OA articles are governed by the applicable Creative Commons License

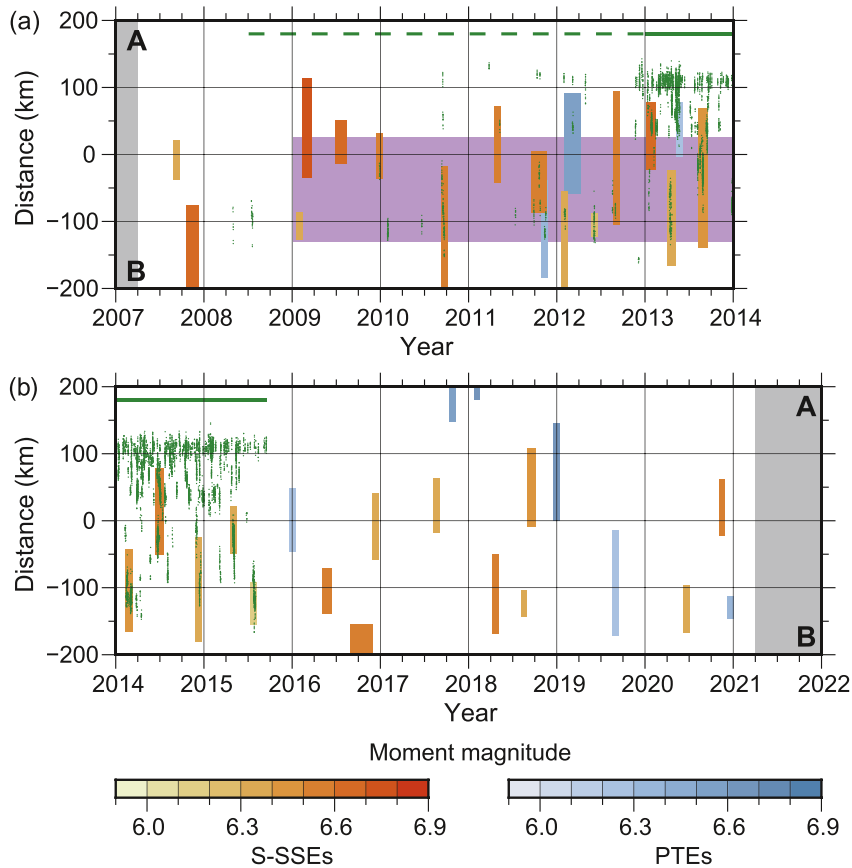

Figure 4. Space-time diagram of S-SSEs, PTEs, and tectonic tremors. The x- and y-axes are time and distance along the A-B line (Figure 2a), respectively. The warm- and cold-colored rectangles and green dots represent S-SSEs, PTEs, and tremors (Wech, 2016), respectively. The purple rectangle represents the approximate location of the 2009–2013 Upper Cook Inlet L-SSE (Rousset, Fu et al., 2019). The contrast of rectangles shows the moment magnitude of each S-SSE. The length and width of the rectangles show the projected distance and duration of the detected events, although the minimum plotted width is 25 days even for the event with a duration of less than 25 days for visualization. The dashed and solid green lines represent the period of the tremor catalog before and after the upgrade of a seismic network, respectively.

3.4. Comparison of S-SSEs to Other Aseismic Slips on the Plate Interface

At the down-dip extension of the 1964 earthquake rupture zone, the afterslip was estimated using geodetic data from leveling, tide gauge, and GNSS observations (e.g., Suito & Freymueller, 2009). We found that the location of the western S-SSE cluster (indicated as "W" in Figure 2b) corresponded to that of the maximum peak of the afterslip (Suito & Freymueller, 2009). The occurrence of SSEs in the afterslip region of the 1964 earthquake has been reported by previous studies (e.g., Suito & Freymueller, 2009), and the co-location between SSEs and afterslip has also been observed in the Nankai subduction zone (Sherrill & Johnson, 2021; Yarai & Ozawa, 2013). However, no studies, including our present study, have detected significant SSEs near Kodiak Island, where the large coseismic slip and afterslip were estimated (e.g., Christensen & Beck, 1994; Suito & Freymueller, 2009). We consider that the difference in whether SSEs spatially coincide with the afterslip relates to the along-trench variation of a physical condition related to the Yakutat microplate, as discussed previously. We also suspect that the western S-SSE cluster was activated by coseismic slip and afterslip of the 1964 Alaska earthquake.

The source area of the S-SSEs was close to that of the L-SSEs in southcentral Alaska. The detected S-SSEs can be interpreted as slip acceleration of the LCI L-SSEs, as discussed in Section 3.2. In the case of the UCI L-SSEs, the two major S-SSE clusters were located on both along-strike sides of the L-SSEs source area (Figure 2b) (e.g., Fu et al., 2015). The L-SSEs source area overlapped that of S-SSEs in a deep part but extended beyond that of S-SSEs in a shallow portion (Figure 2b). Major S-SSE activity is often observed at the down-dip portion of large L-SSEs in the Nankai (e.g., Hirose & Obara, 2005) and Mexican subduction zones (e.g., Frank et al., 2015). In

19448007, 2023, 17, Downloaded from https://agupubs.onlinelibrary.wiley.com/doi/10.1029/2023GL104901 by Cochrane Japan, Wiley Online Library on [29/11/2023]. See the Terms and Conditions (https://onlinelibrary.wiley.com/terms-and-conditions) on Wiley Online Library for rules of use; OA articles are governed by the applicable Creative Commons License

19448007, 2023, 17, Downloaded from https://agupubs.onlinelibrary.wiley.com/doi/10.1029/2023GL104901 by Cochrane Japan, Wiley Online Library on [29/11/2023]. See the Terms and Conditions (https://onlinelibrary.wiley.com/terms-and-conditions) on Wiley Online Library for rules of use; OA articles are governed by the applicable Creative Commons License

the Nankai subduction zone, the activation of S-SSEs during up-dip L-SSEs has been reported (e.g., Hirose & Obara, 2005). Frank et al. (2018) indicated that the 2006 Guerrero L-SSE in Mexico could be interpreted as a cluster of small S-SSEs. However, we did not find a significant increase in both S-SSEs and tremors (Wech, 2016) during the 2009–2013 UCI L-SSE (Figure 4). This indicates that the temporal relationship between S-SSEs and L-SSEs in southcentral Alaska differs from those in Nankai and Mexico. Rousset, Fu et al. (2019) proposed two end-member models for the relationship between S-SSEs and UCI L-SSEs: (a) the UCI L-SSE is composed of a cluster of S-SSEs, and (b) the L-SSE and S-SSEs are distinctive phenomena and the L-SSE occurs in the up-dip of S-SSEs. Those authors also expected that more frequent and/or energetic S-SSEs would be observed during the L-SSE period in both models. Our findings of the S-SSE and UCI L-SSE relationship prefer the latter model because of their spatial relationship mentioned above. However, no significant change in S-SSE activity was found (Figures 2b and 4). An improvement in the analysis method for SSEs with a wide range of duration can provide clues to quantitatively clarify the interplay between S-SSEs and L-SSEs.

4. Conclusions

We applied an S-SSE systematic detection method to 14 years of GNSS data from southcentral Alaska and successfully detected 31 S-SSEs and 20 potential transient events. The detected S-SSEs were located at a depth from 35 to 45 km, which corresponds to the down-dip extension of the 1964 Alaska earthquake rupture zone. Most S-SSEs were detected northeast of Cook Inlet where the Yakutat microplate subducts, and they were clustered in two areas. We suggest that the S-SSE genesis correlates with the subducting microplate, similar to that of tectonic tremors in southcentral Alaska. Active S-SSEs significantly reduce stress in the source area and transfer it to the up-dip area. The source area of S-SSEs partly overlapped that of L-SSEs and the afterslip caused by the 1964 earthquake, with several S-SSEs occurring during duration of the 2009–2013 L-SSE. The spatial correspondence among different aseismic slips may indicate complex physical conditions at the plate boundary. Future detailed and quantitative analyses will improve our understanding of aseismic slip activity, including S-SSEs in southcentral Alaska.

Data Availability Statement

The source parameter list of all detected events in this study (Table S5 in Supporting Information S1) is available online (https://doi.org/10.5281/zenodo.8259965). The daily coordinates used in our study were provided by the Nevada Geodetic Laboratory (http://geodesy.unr.edu/NGLStationPages/GlobalStationList). The RINEX files are available on the web pages of UNAVCO (https://data.unavco.org/archive/gnss/rinex/obs/) and the National Geodetic Survey (https://geodesy.noaa.gov/corsdata/rinex/) (Table S6 in Supporting Information S1). Both pages consist of yearly subdirectories and daily sub-subdirectories, and daily RINEX files are stored in the daily sub-subdirectory. Note that the UNAVCO web page requires a user account to access the data set. You will need to create an account by registering your name, mail address, country, work sector, and institution on the web registration form. The ANSS Comprehensive Earthquake Catalog is available on the U.S. Geological Survey (USGS) webpage (https://earthquake.usgs.gov/earthquakes/search/). The slab2 model (Hayes et al., 2018) is also available on the USGS website (Hayes, 2018, https://www.sciencebase.gov/catalog/item/5aa1b00ee4b0b1c392e86467/). All figures were created using Generic Mapping Tools version 5.4 (Wessel et al., 2013).

Acknowledgments

We appreciate Dr. Aaron Wech for sharing the tectonic tremor catalog. We are grateful for the helpful comments from Dr. Baptiste Rousset and one anonymous reviewer. Discussions with Dr. Tomoaki Nishikawa improved the quality of this study. This study used GNSS stations installed by UNAVCO, Alaska University Fairbanks, the United States Coast Guard, the Alaska Volcano Observatory, the Federal Aviation Administration, and the National Oceanic and Atmospheric Administration. This work was supported by Japan Science and Technology Agency, the establishment of university fellowships towards the creation of science technology innovation, Grant JPMJFS2123, as well as JSPS (Japan Society for the Promotion of Science) KAKENHI Grant JP21K03702, and the MEXT (Ministry of Education, Culture, Sports, Science, and Technology) of Japan under its The Second Earthquake and Volcano Hazards Observation and Research Program.

References

Akaike, H. (1974). A new look at the statistical model identification. *IEEE Transactions on Automatic Control*, *19*(6), 716–723. https://doi.org/10.1109/TAC.1974.1100705

Beroza, G. C., & Ide, S. (2011). Slow earthquakes and nonvolcanic tremor. *Annual Review of Earth and Planetary Sciences*, *39*(1), 271–296. https://doi.org/10.1146/annurev-earth-040809-152531

Bird, P. (2003). An updated digital model of plate boundaries. *Geochemistry, Geophysics, Geosystems*, *4*(3), 1027. https://doi.org/10.1029/2001GC000252

Blewitt, G., Hammond, W. C., & Kreemer, C. (2018). Harnessing the GPS data explosion for interdisciplinary science. *Eos*, *99*. https://doi.org/10.1029/2018EO104623

Christensen, D. H., & Beck, S. L. (1994). The rupture process and tectonic implications of the great 1964 Prince William Sound earthquake. *Pure and Applied Geophysics*, *142*(1), 29–53. https://doi.org/10.1007/BF00875967

DeMets, C., Gordon, R. G., & Argus, D. F. (2010). Geologically current plate motions. *Geophysical Journal International*, *181*, 1–80. https://doi.org/10.1111/j.1365-246X.2009.04491.x

Dragert, H., Wang, K., & James, T. S. (2001). A silent slip event on the deeper Cascadia subduction interface. *Science*, *292*(5521), 1525–1528. https://doi.org/10.1126/science.1060152

Eberhart-Phillips, D., Christensen, D. H., Brocher, T. M., Hansen, R., Ruppert, N. A., Haeussler, P. J., & Abers, G. A. (2006). Imaging the transition from Aleutian subduction to Yakutat collision in central Alaska, with local earthquakes and active source data. *Journal of Geophysical Research*, *111*(B11), B11303. https://doi.org/10.1029/2005JB004240

Elliott, J. L., Larsen, C. F., Freymueller, J. T., & Motyka, R. J. (2010). Tectonic block motion and glacial isostatic adjustment in southeast Alaska and adjacent Canada constrained by GPS measurements. *Journal of Geophysical Research*, *115*(B9), B09407. https://doi.org/10.1029/2009JB007139

Frank, W. B., Radiguet, M., Rousset, B., Shapiro, N. M., Husker, A. L., Kostoglodov, V., et al. (2015). Uncovering the geodetic signature of silent slip through repeating earthquakes. *Geophysical Research Letters*, *42*(8), 2774–2779. https://doi.org/10.1002/2015GL063685

Frank, W. B., Rousset, B., Lasserre, C., & Campillo, M. (2018). Revealing the cluster of slow transients behind a large slow slip event. *Science Advances*, *4*(5), eaat066. https://doi.org/10.1126/sciadv.aat0661

Fu, Y., Liu, Z., & Freymueller, J. T. (2015). Spatiotemporal variations of the slow slip event between 2008 and 2013 in the southcentral Alaska subduction zone. *Geochemistry, Geophysics, Geosystems*, *16*(7), 2450–2461. https://doi.org/10.1002/2015GC005904

Hayes, G. (2018). *Slab2 - A comprehensive subduction zone geometry model*. U.S. Geological Survey data release. https://doi.org/10.5066/F7PV6JNV

Hayes, G. P., Moore, G. L., Portner, D. E., Hearne, M., Flamme, H., Furtney, M., & Smoczyk, G. M. (2018). Slab2, a comprehensive subduction zone geometry model. *Science*, *362*(6410), 58–61. https://doi.org/10.1126/science.aat4723

Hirose, H., Hirahara, K., Kimata, F., Fujii, N., & Miyazaki, S. (1999). A slow thrust slip event following the two 1996 Hyuganada Earthquakes beneath the Bungo Channel, southwest Japan. *Geophysical Research Letters*, *26*(21), 3237–3240. https://doi.org/10.1029/1999GL010999

Hirose, H., & Obara, K. (2005). Repeating short- and long-term slow slip events with deep tremor activity around the Bungo channel region, southwest Japan. *Earth Planets and Space*, *57*(10), 961–972. https://doi.org/10.1186/BF03351875

Ide, S., Beroza, G., Shelly, D., & Uchide, T. (2007). A scaling law for slow earthquakes. *Nature*, *447*(7140), 76–79. https://doi.org/10.1038/nature05780

Iwamoto, K., Suenaga, N., & Yoshioka, S. (2022). Relationship between tectonic tremors and 3-D distributions of thermal structure and dehydration in the Alaska subduction zone. *Scientific Reports*, *12*(1), 6234. https://doi.org/10.1038/s41598-022-10113-2

Kim, Y., Abers, G. A., Li, J., Christensen, D., Calkins, J., & Rondenay, S. (2014). Alaska Megathrust 2: Imaging the megathrust zone and Yakutat/Pacificplate interface in the Alaska subduction zone. *Journal of Geophysical Research: Solid Earth*, *119*(3), 1924–1941. https://doi.org/10.1002/2013JB010581

Li, H., Wei, M., Li, D., Liu, Y., Kim, Y., & Zhou, S. (2018). Segmentation of slow slip events in south central Alaska possibly controlled by a subducted oceanic plateau. *Journal of Geophysical Research: Solid Earth*, *123*(1), 418–436. https://doi.org/10.1002/2017JB014911

Li, S., Freymueller, J., & McCaffrey, R. (2016). Slow slip events and time-dependent variations in locking beneath Lower Cook Inlet of the Alaska-Aleutian subduction zone. *Journal of Geophysical Research: Solid Earth*, *121*(2), 1060–1079. https://doi.org/10.1002/2015JB012491

Michel, S., Gualandi, A., & Avouac, J. (2019a). Interseismic coupling and slow slip events on the Cascadia megathrust. *Pure and Applied Geophysics*, *176*(9), 3867–3891. https://doi.org/10.1007/s00024-018-1991-x

Michel, S., Gualandi, A., & Avouac, J. P. (2019b). Similar scaling laws for earthquakes and Cascadia slow-slip events. *Nature*, *574*(7779), 522–526. https://doi.org/10.1038/s41586-019-1673-6

Nishimura, T. (2014). Short-term slow slip events along the Ryukyu Trench, southwestern Japan, observed by continuous GNSS. *Progress in Earth and Planetary Science*, *1*, 22. https://doi.org/10.1186/s40645-014-0022-5

Nishimura, T., Matsuzawa, T., & Obara, K. (2013). Detection of short-term slow slip events along the Nankai Trough, southwest Japan, using GNSS data. *Journal of Geophysical Research: Solid Earth*, *118*(6), 3112–3125. https://doi.org/10.1002/jgrb.50222

Obara, K. (2002). Nonvolcanic deep tremor associated with subduction in southwest Japan. *Science*, *296*(5573), 1679–1681. https://doi.org/10.1126/science.1070378

Obara, K., Hirose, H., Yamamizu, F., & Kasahara, K. (2004). Episodic slow slip events accompanied by non-volcanic tremors in southwest Japan subduction zone. *Geophysical Research Letters*, *31*(23), L23602. https://doi.org/10.1029/2004GL020848

Obara, K., & Sekine, S. (2009). Characteristic activity and migration of episodic tremor and slow-slip events in central Japan. *Earth Planets and Space*, *61*(7), 853–862. https://doi.org/10.1186/BF03353196

Ohta, Y., Freymueller, J. T., Hreinsdóttir, S., & Suito, H. (2006). A large slow slip event and the depth of the seismogenic zone in the south central Alaska subduction zone. *Earth and Planetary Science Letters*, *247*(1–2), 108–116. https://doi.org/10.1016/j.epsl.2006.05.013

Ohzono, M., Takahashi, H., & Ichiyanagi, M. (2015). An intraplate slow earthquake observed by a dense GPS network in Hokkaido, northernmost Japan. *Geophysical Journal International*, *200*(1), 144–148. https://doi.org/10.1093/gji/ggu380

Okada, Y. (1992). Internal deformation due to shear and tensile faults in a half-space. *Bulletin of the Seismological Society of America*, *82*(2), 1018–1040. https://doi.org/10.1785/BSSA0820021018

Okada, Y., Nishimura, T., Tabei, T., Matsushima, T., & Hirose, H. (2022). Development of a detection method for short-term slow slip events using GNSS data and its application to the Nankai subduction zone. *Earth Planets and Space*, *74*(1), 18. https://doi.org/10.1186/s40623-022-01576-8

Ozawa, S., Miyazaki, S., Hatanaka, Y., Imakiire, T., Kaidzu, M., & Murakami, M. (2003). Characteristic silent earthquakes in the eastern part of the Boso peninsula, Central Japan. *Geophysical Research Letters*, *30*(6), 1283. https://doi.org/10.1029/2002GL016665

Plattner, C., Malservisi, R., Dixon, T. H., LaFemina, P., Sella, G. F., Fletcher, J., & Suarez-Vidal, F. (2007). New constraints on relative motion between the Pacific Plate and Baja California microplate (Mexico) from GPS measurements. *Geophysical Journal International*, *170*(3), 1373–1380. https://doi.org/10.1111/j.1365-246X.2007.03494.x

Rogers, G., & Dragert, H. (2003). Episodic tremor and slip on the Cascadia subduction zone: The chatter of silent slip. *Science*, *300*(5627), 1942–1943. https://doi.org/10.1126/science.1084783

Rousset, B., Bürgmann, R., & Campillo, M. (2019). Slow slip events in the roots of the San Andreas fault. *Science Advances*, *5*(2), eaav3274. https://doi.org/10.1126/sciadv.aav3274

Rousset, B., Campillo, M., Lasserre, C., Frank, W. B., Cotte, N., Walpersdorf, A., et al. (2017). A geodetic matched filter search for slow slip with application to the Mexico subduction zone. *Journal of Geophysical Research: Solid Earth*, *122*(12), 10498–10514. https://doi.org/10.1002/2017JB014448

Rousset, B., Fu, Y., Bartlow, N. M., & Bürgmann, R. (2019). Weeks-long and years-long slow slip and tectonic tremor episodes on the south central Alaska megathrust. *Journal of Geophysical Research: Solid Earth*, *124*(12), 13392–13403. https://doi.org/10.1029/2019JB018724

Schwartz, S. Y., & Rokosky, J. M. (2007). Slow slip events and seismic tremor at circum-pacific subduction zones. *Reviews of Geophysics*, *45*(3), RG3004. https://doi.org/10.1029/2006RG000208

Sherrill, E. M., & Johnson, K. M. (2021). New insights into the slip budget at Nankai: An iterative approach to estimate coseismic slip and afterslip. *Journal of Geophysical Research: Solid Earth*, *126*(2), e2020JB020833. https://doi.org/10.1029/2020JB020833

19448007, 2023, 17, Downloaded from https://agupubs.onlinelibrary.wiley.com/doi/10.1029/2023GL104901 by Cochrane Japan, Wiley Online Library on [29/11/2023]. See the Terms and Conditions (https://onlinelibrary.wiley.com/terms-and-conditions) on Wiley Online Library for rules of use; OA articles are governed by the applicable Creative Commons License

Suito, H., & Freymueller, J. T. (2009). A viscoelastic and afterslip postseismic deformation model for the 1964 Alaska earthquake. *Journal of Geophysical Research*, *114*(B11), B11404. https://doi.org/10.1029/2008JB005954

U.S. Geological Survey, & Alaska Department of Natural Resources. (2021). Quaternary fault and fold database for the United States. Retrieved from https://www.usgs.gov/natural-hazards/earthquake-hazards/faults

Vallée, M., Nocquet, J. M., Battaglia, J., Font, Y., Segovia, M., Régnier, M., et al. (2013). Intense interface seismicity triggered by a shallow slow slip event in the Central Ecuador subduction zone. *Journal of Geophysical Research: Solid Earth*, *118*(6), 2635–3273. https://doi.org/10.1002/jgrb.50216

Wallace, L. M. (2020). Slow slip events in New Zealand. *Annual Review of Earth and Planetary Sciences*, *48*(1), 175–203. https://doi.org/10.1146/annurev-earth-071719-055104

Wdowinski, S., Bock, Y., Zhang, J., Fang, P., & Genrich, J. (1997). Southern California permanent GPS geodetic array: Spatial filtering of daily positions for estimating coseismic and postseismic displacements induced by the 1992 Landers earthquake. *Journal of Geophysical Research*, *102*(B8), 18057–18070. https://doi.org/10.1029/97JB01378

Wech, A. G. (2016). Extending Alaska's plate boundary: Tectonic tremor generated by Yakutat subduction. *Geology*, *44*(7), 587–590. https://doi.org/10.1130/G37817.1

Wech, A. G., & Bartlow, N. M. (2014). Slip rate and tremor genesis in Cascadia. *Geophysical Research Letters*, *41*(2), 392–398. https://doi.org/10.1002/2013GL058607

Weerasinghe, D., & Fu, Y. (2021). Short-term slow slip events at Alaska subduction zone and their correlation with local tremors. In *Abstract T54A-05 presented at 2021 fall meeting*. AGU.

Wei, M., McGuire, J. J., & Richardson, E. (2012). A slow slip event in the south central Alaska Subduction Zone and related seismicity anomaly. *Geophysical Research Letters*, *39*(15), L15309. https://doi.org/10.1029/2012GL052351

Wessel, P., Smith, W. H. F., Scharroo, R., Luis, J., & Wobbe, F. (2013). Generic mapping tools: Improved version released. *Eos, Transactions, American Geophysical Union*, *94*(45), 409–410. https://doi.org/10.1002/2013EO450001

Yarai, H., & Ozawa, S. (2013). Quasi-periodic slow slip events in the afterslip area of the 1996 Hyuga-nada earthquakes, Japan. *Journal of Geophysical Research: Solid Earth*, *118*(5), 2512–2527. https://doi.org/10.1002/jgrb.50161

References From the Supporting Information

Cleveland, R. B., Cleveland, W. S., McRae, J. E., & Terpenning, I. (1990). STL: A seasonal-trend decomposition procedure based on loess. *Journal of Official Statistics*, *6*(1), 3–73.

Matsu'ura, M., & Hasegawa, Y. (1987). A maximum likelihood approach to nonlinear inversion under constraints. *Physics of the Earth and Planetary Interiors*, *47*, 179–187. https://doi.org/10.1016/0031-9201(87)90076-8

Okada, Y. (1995). Simulated empirical law of coseismic crustal deformation. *Journal of Physics of the Earth*, *43*(6), 697–713. https://doi.org/10.4294/jpe1952.43.697

19448007, 2023, 17, Downloaded from https://agupubs.onlinelibrary.wiley.com/doi/10.1029/2023GL104901 by Cochrane Japan, Wiley Online Library on [29/11/2023]. See the Terms and Conditions (https://onlinelibrary.wiley.com/terms-and-conditions) on Wiley Online Library for rules of use; OA articles are governed by the applicable Creative Commons License